*polymers*

MDPI

*Article*

# Gamma Irradiation-Induced Changes in Microstructure of Cyclic Olefin Copolymer (COC) Revealed by NMR and SAXS Characterization

**Fan Zhang [1,2], Heng Lei [1,2,3], Feng Guo [1,2], Jiangtao Hu [1,2], Haiming Liu [3], Qing Wang [3], Weihua Liu [1,2], Zhe Xing [1,2,*] and Guozhong Wu [1,2,3,*]**

[1] Shanghai Institute of Applied Physics, Chinese Academy of Sciences, No. 2019 Jialuo Road, Jiading District, Shanghai 201800, China
[2] University of Chinese Academy of Sciences, Beijing 100049, China
[3] School of Physical Science and Technology, ShanghaiTech University, Shanghai 201210, China
* Correspondence: xingzhe@sinap.ac.cn (Z.X.); wuguozhong@sinap.ac.cn (G.W.); Tel.: +86-21-39194630; (Z.X.); +86-21-39194531 (G.W.)

**Abstract**

Cyclic Olefin Copolymer (COC) is an amorphous thermoplastic polymer synthesized through the catalytic copolymerization of α-olefin and cyclic olefin. When used in pre-filled syringes and pharmaceutical packaging, COCs require radiation sterilization. The radiation sterilization alters the microstructure of COC, which ultimately affects its performance and biosafety. In this study, to investigate the effects of γ-radiation on COC microstructures, ethylene-norbornene copolymers with various compositions, representative of COC, are studied by nuclear magnetic resonance (NMR) and small angle X-ray scattering (SAXS) techniques. During irradiation, the COC containing 35 mol% norbornene produced free radicals that triggered migration and reaction processes, leading to the formation of entanglements within flexible chain segments. This, in turn, affected nearby ring structures with high steric hindrance, resulting in a 9.2% decrease in internal particle size and an increase in particle spacing. Conversely, when the norbornene content in COC was increased to 57 mol%, the internal particle size increased by 17.9%, while the particle spacing decreased.

**Keywords:** cyclic olefin copolymer; microstructure; gamma radiation; NMR; SAXS

check for updates

Academic Editor: Ian Wyman

Received: 9 May 2025
Revised: 22 June 2025
Accepted: 23 June 2025
Published: 24 June 2025

**Citation:** Zhang, F.; Lei, H.; Guo, F.; Hu, J.; Liu, H.; Wang, Q.; Liu, W.; Xing, Z.; Wu, G. Gamma Irradiation-Induced Changes in Microstructure of Cyclic Olefin Copolymer (COC) Revealed by NMR and SAXS Characterization. *Polymers* **2025**, *17*, 1751. https://doi.org/10.3390/polym17131751

**Copyright:** © 2025 by the authors. Licensee MDPI, Basel, Switzerland. This article is an open access article distributed under the terms and conditions of the Creative Commons Attribution (CC BY) license (https://creativecommons.org/licenses/by/4.0/).

## 1. Introduction

Cyclic Olefin Copolymer (COC) is a class of polymers synthesized through the catalytic addition polymerization of norbornene or its derivatives as the primary monomer, combined with α-olefins as comonomers [1–3]. COCs are high-quality, transparent thermoplastic engineering plastics. Among these, ethylene-norbornene copolymers have gained significant attention due to their appealing properties and were commercialized under the trade name TOPAS by German Ticona in 2000. The properties of these materials can be finely turned by adjusting the molar ratio of norbornene during polymerization. These innovative commercial materials boast a unique combination of performance advantages, including variable glass transition temperatures ranging from 65 °C to 178 °C, heat resistance, chemical resistance to common solvents, low moisture absorption, high water barrier properties, excellent mechanical strength, ease of extrusion and thermoforming, compatibility with polyolefin, and exceptional biocompatibility and inertia. These numerous benefits have led to their widespread application in medical devices and packaging materials, for which COCs must undergo rigorous sterilization processes to ensure sterility and safety. γ-Ray sterilization is one of the most commonly used methods, as commercially

successful technologies have been developed that enable the rapid sterilization of a wide range of disposable medical devices. However, the effects of irradiation sterilization on the properties of polymer materials are unavoidable. The high-energy electrons generated during the irradiation process are known to create reaction intermediates and free radicals within the polymer, which can follow multiple reaction pathways, leading to cross-linking or cleavage [4–7]. These changes can alter the mechanical and surface properties of the polymer. In previous research, we investigated the types of free radicals produced in COC upon exposure to gamma radiation and examined the mechanisms of attenuation, as well as the underlying causes of radiation-induced color changes [8–10]. However, the impact of irradiation on the microstructure of COC remains unclear and requires further research and exploration.

The ethylene-norbornene (E-N) copolymer, which was developed in the late 1950s, falls within this COC category. In 1989, Kaminsky pioneered the synthesis of cyclic olefin polymers notable for their exceptional transparency and high hardness using metallocene catalysts [11]. Different catalysts can facilitate the formation of isotactic or syndiotactic chain structures [12]. By selecting specific catalyst systems, the incorporation of norbornene units can be controlled, allowing for regulation of the copolymer's microstructure and stereoselectivity [13–22]. Recent advancements in polymer characterization have incorporated the use of pentads to represent the stereochemistry of consecutive monomer units, offering deeper insights into the spatial arrangements and chirality within COC chains.

In ethylene (E)-norbornene (N) copolymers, the arrangement of norbornene units results in various structural motifs that significantly influence material properties, including alternating (NENEN), dimeric (ENNE), and trimetic (ENNNE) configurations. Recent research, as illustrated in Figure 1, has also explored the presence of meso and racemic structures within COC chains. Meso compounds are notable for their internal symmetry, which renders the optically inactive despite containing multiple chiral centers. These structures arise from symmetrical planes or centers of symmetry within the molecular framework. In contrast, racemic mixtures consist of equal proportions of two enantiomers—mirror-image molecules that do not optically rotate plane-polarized light. The mechanisms by which irradiation induces structural changes in COCs are not yet fully understood. While existing literature provides valuable insights into the structures of COC chain segments, this study aims to investigate the effects of irradiation on COCs based on these findings.

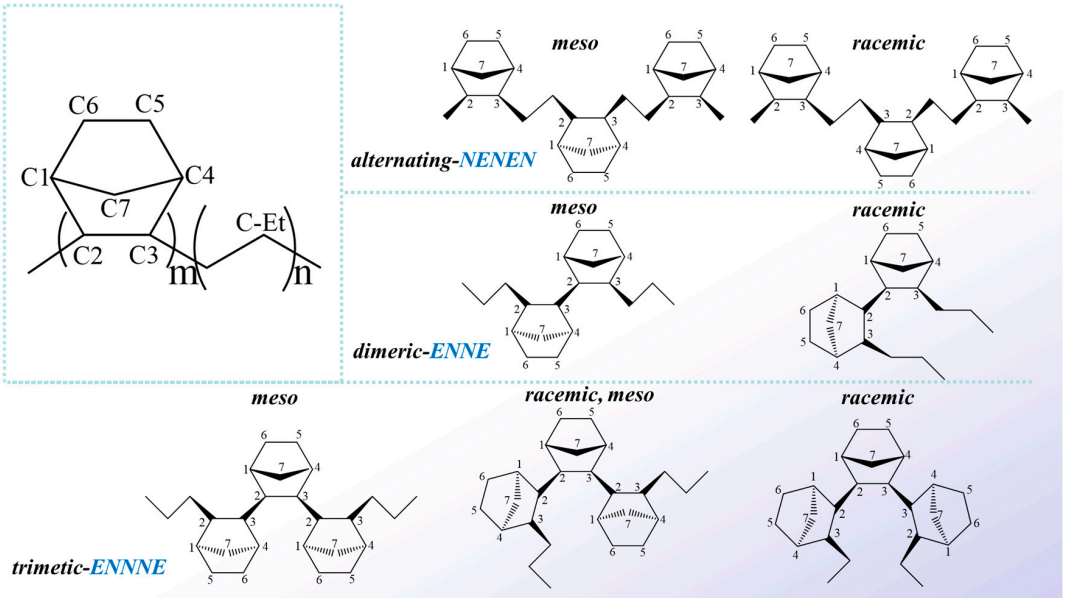



**Figure 1.** Various segments and microstructures in COC.

Nuclear Magnetic Resonance (NMR) spectroscopy, encompassing $^{1}H$, $^{13}C$, and 2D correlation techniques, is undoubtedly one of the most powerful analytical tools for studying polymer microstructures [23]. NMR enables the characterization of electronic shielding, molecular structure, and the presence of functional groups through the analysis of unique chemical shifts, coupling constants, and relaxation times. The carbon numbering of the utilized norbornene aligns with previous studies [24–37], highlighting differences in distribution and ensuring that C1, C2, and C6 are consistently positioned closer to other norbornene units compared to C3, C4, and C5 [27–31]. The spectral assignments of COCs are notably complex, as each norbornene fragment comprises two stereoisomeric five-membered rings, deviating from the straightforward addition rule of chemical shifts.

$^{1}H$ NMR studies [32,33] on COCs with various compositions distinguished hydrogen signal on the ethylene chain segment and on the ring and allowed determination of norbornene content. The norbornene fraction may be calculated using formula (1), where a is the integral sum of the bridging hydrogens (C1-H and C4-H) and b is the rest of the C-H signals, respectively. In addition, the team analyzed the hydrogen atom signals of different environments of COCs using HMQC. The chemical shift analysis of hydrogen is shown in Table 1:

$$\text{Norbornene}(\text{mol}\%) = 2a/(b - 2a) \quad (1)$$

**Table 1.** $^{1}H$ NMR and $^{13}C$ NMR assignments of COC microstructures, including alternating-NENEN, dimeric-ENNE, and trimetic-ENNNE configurations.

| Sequences | | C Chemical Shifts | Reference | H Chemical Shifts | Reference |
|---|---|---|---|---|---|
| C-Et | EEEEE | 27.7 | [27–37] | 0.9–1.5 | |
| | NENEN | 28.0 | | | |
| C5/C6 | ENNE | 26.2 | [27,31–37] | 0.9–1.5 | |
| | ENNE | 29.7 | [27,31–36] | | |
| | NENEN | 28.3 | [27,31–36] | | |
| C7 | NENEN | 31.0 | [27,31–36] | 0.9 | |
| | ENNE | 31.3 | [27,31–36] | 1.4 | |
| C1/C4 | EENEE | 39.5 | [27,31–36] | Not available | [32,33] |
| | NENEN | 39.5 | [27,31–36] | 1.9 | |
| | ENNE | 40.4 | [27,31–36] | 1.8, 2.0 | |
| C2/C3 | NENEN | 45.2 | [27–36] | 1.4 | [32,33] |
| | ENNE | 48.1 | [27–36] | 1.2, 1.4 | |
| | NENNN | 50.8–52.0 | [27,34,36] | Not available | |

Extensive investigations have been conducted on the NMR spectral analysis of ethylene-norbornene copolymers, revealing a significant correlation between the conformational characteristics of these copolymers and their corresponding $^{13}C$ NMR chemical shifts. Notably, critical microstructural features essential for distinguishing isotactic and atactic norbornene sequences were identified and characterized. Furthermore, the influence of monomer concentration on the microstructural evolution of ethylene-norbornene copolymers was systematically investigated. A comprehensive compilation of the $^{13}C$ NMR assignments corresponding to the microstructural elements of COC is also presented in Table 1, providing a detailed reference for structural characterization.

Small-Angle X-ray Scattering (SAXS) is a powerful technique for characterizing the dimensions and morphology of polymer particles and voids, analyzing phase structures in polymer blends, and determining structural features such as long periods, branched chains, molecular chain lengths, and glass transition temperatures. SAXS measures variations in electron density within a material at a scale of 1 to 100 nanometers. When X-rays pass through an ultra-fine powder layer, they are scattered by the electrons in the powder

particles, producing scattering at very small angles relative to the incident beam. The intensity distribution of the scattered X-rays correlates with the size and distribution of the particles. The fundamental principle of SAXS relies on the electron density contrast between the scatterers and the surrounding medium. Despite its advancements in elucidating polymer and composite structures, there is a notable lack of research investigating the effects of irradiation on polymer materials, particularly polymer-based composites, using SAXS. For instance, Hai et al. [38] investigated the structural evolution of HDPE/carbon particle-doped HDPE under 1.157 GeV Fe ion irradiation at varying doses using SAXS. The study revealed that carbon particle doping protected the long-period structure of HDPE, conferring certain radiation resistance to the material. Fayolle et al. [39] systematically studied the structural and property evolution of polyoxymethylene under γ-ray irradiation using SAXS and wide-angle X-ray scattering (WAXS). They discovered two competing mechanisms during irradiation: material degradation caused by molecular chain scission and structural reorganization driven by chemical crystallization. At low absorption doses, molecular rearrangement in amorphous regions promoted secondary crystallization, increasing lamellar thickness and significantly enhancing crystallinity. With higher absorption doses, main chain scission became dominant, leading to reduced molar mass, intensified end-group oxidation, and consequent deterioration of mechanical properties. Somani et al. [40] employed synchrotron radiation SAXS to systematically study the shear-induced crystallization process of isotactic PP in supercooled melt. Analysis of SAXS scattering patterns revealed the formation of highly oriented lamellar structures in isotactic PP under shear flow. Rui [41] treated LDPE/carbon nanotube composites with high-energy (170 keV) electron beam irradiation. Porod theory analysis of SAXS data demonstrated that incorporating carbon nanotubes not only enhanced irradiation stability but also mitigated material degradation by suppressing radical migration, in particular showing excellent mechanical property retention at higher absorption doses.

While extensive research has elucidated the irradiation-dependent macroscopic property evolution of COCs, the fundamental microstructural determinants governing these radiation effects remain underexplored at the molecular scale. By employing an integrated approach combining NMR and SAXS, this work systematically investigates the radiation-induced conformational and structural changes in COC chain segments, providing novel mechanistic insights into the deeper understanding of the radiation properties of COC.

## 2. Materials and Methods

### *2.1. Sample Preparation*

COCs, specifically TOPAS grades 8007, 5013, 6015, and 6017, were evaluated. The norbornene content in each grade of COC is presented in Table 2. COCs were irradiated at a dose rate of 2 kGy/h at room temperature in air, using a $^{60}$Co γ-ray source at the Shanghai Institute of Applied Physics. The total absorbed doses for the specimens were 25 kGy and 100 kGy, respectively.

**Table 2.** Content of norbornene in each COC grade.

| TOPAS Grades | Norbornene/mol% (Reference) | Norbornene/mol% (Sample) | Absorbed Dose (kGy) | Sample |
|---|---|---|---|---|
| 8007 | 35 | 37.5 | 25 | COC-35-25 |
| | | | 100 | COC-35-100 |
| 5013 | 46 | 48.3 | 25 | COC-46-25 |
| | | | 100 | COC-46-100 |
| 6015 | 52 | 52.5 | 25 | COC-52-25 |
| | | | 100 | COC-52-100 |
| 6017 | 57 | 55.5 | 25 | COC-57-25 |
| | | | 100 | COC-57-100 |

### *2.2. Experimental Operation*

Weigh 10–20 mg of the COC sample and dissolve it in deuterated chloroform ($CDCl_3$, 99.9% deuterium purity) to prepare a concentrated solution. All $^1H$ NMR experiments were conducted at room temperature or 50 °C using a Bruker 500 MHz NMR spectrometer (Berlin, Germany) equipped with a 5 mm probe, with tetramethylsilane (TMS) as the internal standard for calibration. All HSQC and $^{13}C$ NMR experiments were performed at room temperature on a Quantum-I Plus 400 MHz NMR spectrometer (Wuhan, China) with a 5 mm probe, using TMS as the internal standard for calibration. The NMR data were processed and analyzed using MestReNova (15.0) software.

SAXS testing of the sample was performed at the BL10U1 station of the Shanghai Synchrotron Radiation Facility. The two-dimensional SAXS scattering pattern was recorded using an Eiger 1M detector (Dectris, Baden-Daettwil, Switzerland) with a pixel size of 79 μm × 79 μm. The X-ray wavelength was 1.24 A and the distance from the sample to the detector was 4500 mm. The data collection time for all samples was set to 1 s. The SAXS curve, depicting the relationship between scattering intensity I(q) and the scattering vector $q = (4\pi/\lambda)\sin\theta$, was calculated using Fit 2D (17.006) software, where λ represents the X-ray wavelength and θ denotes the half-scattering angle.

## 3. Results and Discussion

### *3.1. The Effect of Gamma Radiation on the Segments of COC Analyzed via NMR Spectroscopy*

$^1H$-$^{13}C$ HSQC NMR spectroscopy was employed to elucidate structural correlations between protons and directly bonded carbon nuclei in gamma-irradiated COCs. To investigate radiation-induced modifications, the $^1H$ and $^{13}C$ NMR spectrum of COC-35 were acquired at ambient temperature and analyzed in conjunction with the 2D $^1H$-$^{13}C$ HSQC spectrum, as illustrated in Figure 2, enabling the unambiguous assignment of proton-carbon coupling networks. The key cross-peaks observed in the HSQC spectrum were systematically assigned, as summarized in Table 3, providing critical insights into radiation-induced structural rearrangements at the molecular level.

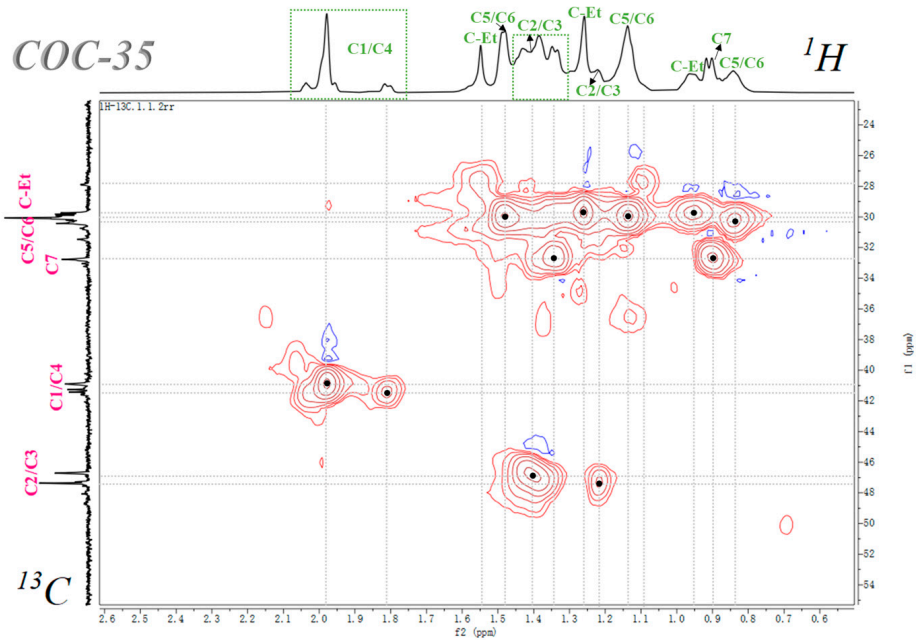



**Figure 2.** The correspondence between the $^1H$ NMR, $^{13}C$ NMR, and HSQC in COC-35. (The spectra were all acquired at room temperature).

**Table 3.** Attribution of cross peaks in $^{1}H$-$^{13}C$ HSQC spectrum of COC-35.

| | H Chemical Shifts | C Chemical Shifts | Sequences | Reference |
|---|---|---|---|---|
| C-Et | 1.0 | 29.6 | EENEE | This work |
| | 1.1 | 29.9 | NENEN | |
| | 1.6 | 27.7 | ENNE | |
| C5/C6 | 0.8 | 30.2 | EENEE | This work |
| | 1.1 | 29.9 | NENEN | |
| | 1.5 | 29.9 | ENNE | |
| C7 | 0.9 | 32.5 | EENEE | This work |
| | 1.3 | 32.5 | ENNE | |
| C1/C4 | 1.8 | 41.5 | NENEN/EENEE | [24] |
| | 2.0 | 40.9 | ENNE | |
| C2/C3 | 1.2 | 47.3 | ENNE | [24] |
| | 1.4 | 47.0 | NENEN/EENEE | |
| | 1.4 | 48.6 | ENNE | |

Subsequent high-temperature NMR measurements significantly improved peak resolution by enhancing molecular chain mobility. Elevated temperatures reduce intermolecular interactions, thereby minimizing peak overlap and broadening effects, which is particularly advantageous for polymer systems. The benefits of high-temperature testing are especially pronounced in polymeric materials, which often exhibit poor solubility or chain entanglement at ambient conditions due to their high molecular weight and complex chain architecture. These factors typically result in weak, broad, or overlapping NMR signals. Heating facilitates solvent penetration and disentanglement of polymer chains, improving sample solubility and promoting more homogeneous molecular dispersion in solution. This leads to enhanced signal intensity and narrower linewidths. Furthermore, increased thermal energy accelerates molecular motion, shortening relaxation times and yielding sharper, more well-defined peaks in the NMR spectra.

The types of free radicals generated in COCs under γ-ray irradiation were analyzed by electron spin resonance (ESR) spectroscopy. Although varying irradiation doses altered the signal intensities in these materials, they did not change the ESR line shapes, indicating that the radical types were independent of the irradiation dose (as shown in Figure S1). Subsequently, changes in the segmental structures after irradiation were examined using $^{1}H$ NMR spectroscopy: COC-35 is shown in Figure 3, COC-46 in Figure S2, COC-52 in Figure S3, and COC-57 in Figure S4.

For COC-35-100, spectral changes at 2.07 ppm (indicating increased ENNE segment content) and decreased integration area at 1.83 ppm (corresponding to reduced EENEE segments) demonstrate radiation-induced crosslinking of flexible chains, which promotes closer spatial arrangement of the cyclic structures.

In ethylene-norbornene copolymers, the terminal methyl group (-$CH_3$) of the ethylene unit typically appears in the $^{1}H$ NMR spectrum within the range of 0.8–1.2 ppm. However, the presence of a ring structure can cause the chemical shift of the terminal group to move upfield (toward a higher field). For instance, the terminal group near a cyclopropane ring exhibits such an upfield shift [42]. Notably, the appearance of a signal at 0.71 ppm in COC-35-100 and COC-46-100 (refer to Figure 4a,b) suggests that irradiation may induce entanglement of the COC copolymer molecular chains, bringing norbornene units into closer proximity. This proximity could lead to a slight upfield shift of the bridgehead hydrogen signal to 0.71 ppm. Additionally, branching reactions in the flexible segments of

the copolymer may also contribute to the appearance of a terminal methyl hydrogen (-$CH_3$) signal at 0.71 ppm.

| Integration | | | | | | | | | | | | | | |
|---|---|---|---|---|---|---|---|---|---|---|---|---|---|---|
| 1 | 2 | 3 | 4 | 5 | 6 | 7 | 8 | 9 | 10 | 11 | 12 | 13 | 14 | 15 |
| COC-35-0 | | | | | | | | | | | | | | |
| 0.32 | 0.56 | 1.08 | 7.92 | 1.99 | 11.25 | 15.88 | 9.24 | 11.03 | 3.53 | 14.14 | 5.25 | 5.64 | 4.28 | |
| COC-35-100 | | | | | | | | | | | | | | |
| 0.02 | 0.39 | 1.53 | 8.30 | 1.34 | 9.40 | 15.85 | 9.79 | 11.61 | 6.30 | 14.29 | 4.85 | 5.17 | 5.50 | 0.60 |

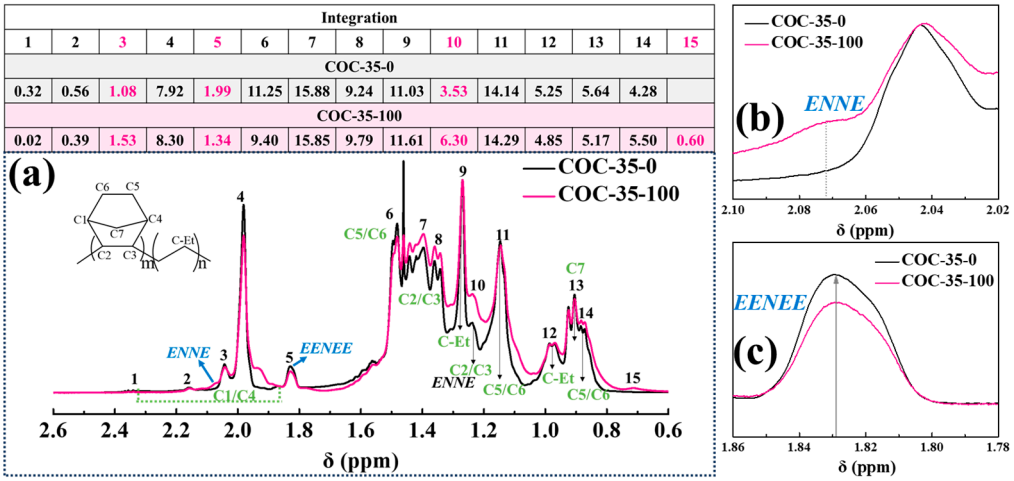



**Figure 3.** (**a**) Comparative analysis of $^1$H NMR (measured at 50 °C) spectral assignments for COC-35 pre- and post-irradiation. The relative integral area for each signal (normalized to total spectral integral of 100%) is tabulated above the corresponding spectra, with signal variations at 2.07 ppm (**b**) and 1.83 ppm (**c**).

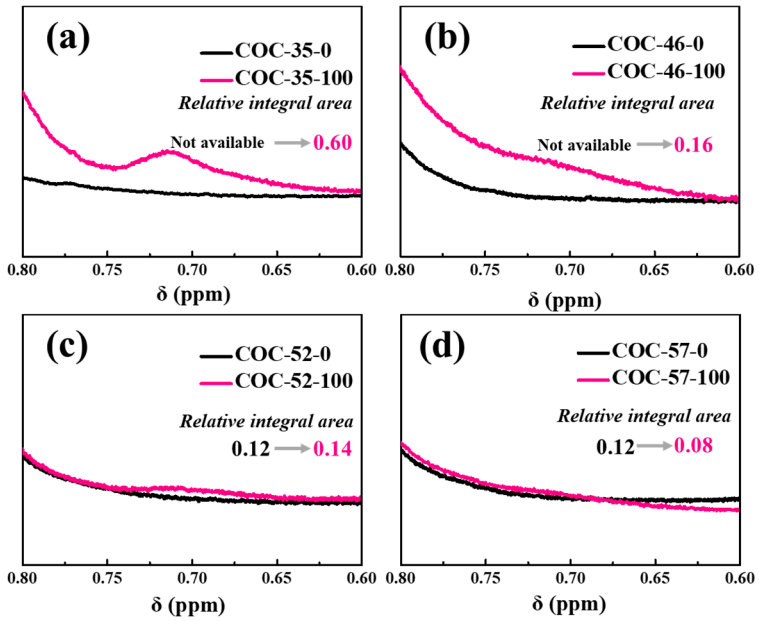



**Figure 4.** $^1$H NMR spectra of (**a**) COC-35, (**b**) COC-46, (**c**) COC-52, and (**d**) COC-57 before and after irradiation: signal variation at 0.71 ppm.

For high-norbornene COC variants, irradiation produces stabilized radicals within sterically hindered chain segments. The restricted mobility of these radicals due to the material's inherent rigidity prevents efficient recombination, ultimately yielding low-molecular-weight degradation products. This behavior stems from the competing processes of rigid-segment stabilization versus flexible-segment crosslinking, with the balance directly influencing the 0.71 ppm signal intensity. While COC-52-100 exhibits a minor integration increase (0.12 to 0.14), COC-57-100 paradoxically shows reduced intensity (0.12 to 0.08; Figure 4c,d), demonstrating how norbornene content dictates radiation response through steric and mobility effects. Temperature-induced chain mobility also reveals structural modifications through differential scanning calorimetry (DSC) analysis (Figure S5). For

irradiated COC-35, the observed increase in $T_g$ indicates the formation of higher-molecular-weight products that restrict chain mobility. In contrast, systems with higher norbornene content exhibit radiation-induced oxidative degradation, generating lower-molecular-weight fragments. These shorter chains demonstrate greater mobility, manifested by a downward shift in $T_g$. This dichotomy highlights how composition-dependent radiation responses govern the thermal-mechanical properties of COC materials.

As the norbornene content increases, the spectral complexity intensifies, potentially leading to overlap in the regions. Longer norbornene sequences may result in signal splitting and shifting, making it challenging to accurately determine the specific content of cyclic structures. To examine the effect of irradiation on the chain structure of COC, this study compared the $^{13}C$ NMR spectra of COCs before and after irradiation at an absorbed dose of 100 kGy, as illustrated in Figure 5. In COC-35-100 (as shown in Figure 5a), the ethylene segment content increased following irradiation. The integral area of C-Et on the EEEEE also increased, indicating that the molecular chains had become twisted and entangled post irradiation, causing the ring structures to move closer together, resulting in stronger peak strengths.

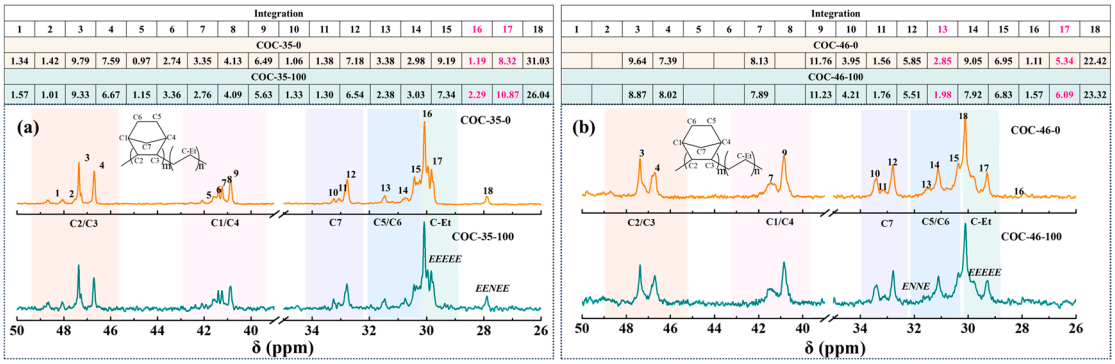



**Figure 5.** Comparative analysis of $^{13}C$ NMR spectral assignments for COC-35 (**a**) and COC-46 (**b**) pre- and post-irradiation. The relative integral area for each signal (normalized to total spectral integral of 100%) is tabulated above the corresponding spectra.

In the case of sample COC-46 (as shown in Figure 5b), although the signal at ethylene segment showed a slight increased post-irradiation, the ENNE segments decreased.

In Figure 6a, the integral area of NENEN segment in COC-52-100 represented by peak 8 showed an increasing trend. When the norbornene content in COC was increased to 57 mol%, notable changes in peak intensities were observed after irradiation (as shown in Figure 6b). Among these changes, the peak intensities corresponding to the peak 18 and 17 of the ethylene segment showed a significant increase. Similarly, the relative integration areas of the peak 4 in the C2/C3 region and the peak 9 position in the C1/C4 region also increased, suggesting a notable enhancement in the signal intensity of NENEN fragments following irradiation. In contrast, the integration value of the peak 14 position in the C5/C6 region was significantly reduced, indicating a weakening of the signal intensity associated with the ENNE segment. Collectively, these observations imply that the tertiary alkyl radicals within the norbornene ring exhibit limited migratory capacity, resulting in their oxidation or rearrangement into low-molecular-weight products characterized by short-chain segments. This behavior stands in contrast to the irradiation-induced entanglement and branching observed in the flexible chain segments of COC-35-100 and COC-46-100.

These observations collectively demonstrate that the tert-alkyl radicals within the norbornene rings exhibit restricted migration capability, ultimately leading to their oxidation or rearrangement into low-molecular-weight products characterized by short-chain segments. This phenomenon stands in stark contrast to the radiation-induced entanglement and

branching observed in the flexible chain segments of COC-35. Furthermore, the findings corroborate earlier FTIR studies showing that increased norbornene content across the four samples significantly enhanced the generation of cyclized radicals upon irradiation [9]. Due to pronounced steric hindrance effects, these radicals displayed constrained mobility and were consequently converted into stable oxidation products, as evidenced by (1) markedly intensified characteristic peaks of carbonyl groups (-C=O) at 1725 $cm^{-1}$ and 1452 $cm^{-1}$ and (2) enhanced post-irradiation signals at 1257 $cm^{-1}$ (tertiary alcohol) and 1095 $cm^{-1}$ (secondary alcohol).

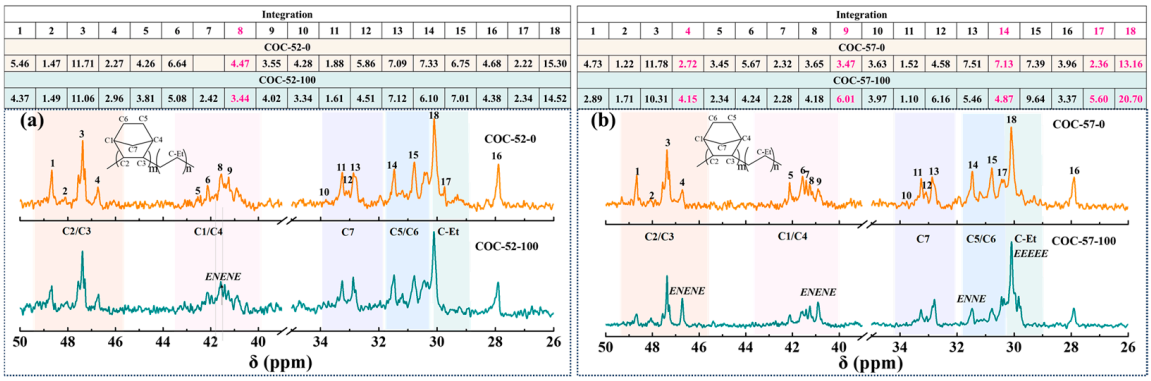



**Figure 6.** Comparative analysis of $^{13}C$ NMR spectral assignments for COC-52 (**a**) and COC-57 (**b**) pre- and post-irradiation. The relative integral area for each signal (normalized to total spectral integral of 100%) is tabulated above the corresponding spectra.

The analysis results of $^{1}H$ NMR and $^{13}C$ NMR indicate that the C-H or C-C bonds in the COC structure break during irradiation, generating alkyl radicals. Due to the significant steric hindrance around the tertiary carbon-centered radicals, the kinetics of their further reactions are limited. In contrast, secondary carbon radicals exhibit higher reactivity because of their lower steric hindrance, making them more prone to coupling reactions with other radicals, which leads to a notable decrease in their signal intensity.

By comparing the COC structure before and after irradiation using $^{1}H$ NMR and $^{13}C$ NMR, it was found that the flexible chain segments can migrate and form entangled structures after irradiation. As the norbornene content increases, the mobility of the cyclic structures decreases, resulting in a relative reduction in the norbornene dimer structures in COC after irradiation, making the segments more susceptible to degradation (as shown in Figure 7).

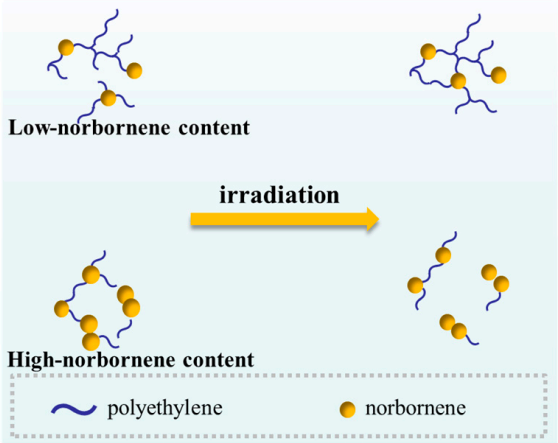



**Figure 7.** Description of chain segment changes after COC irradiation with different norbornene content.

### *3.2. The Effect of Gamma Radiation on Particles Inside COC Analyzed by SAXS*

Additionally, SAXS analysis was employed to compare particle mobility in COC after irradiation. The SAXS diagram of COC exposed to various radiation doses is shown in Figure 8, with the abscissa representing the scattering vector q and the ordinate indicating the scattering intensity I.

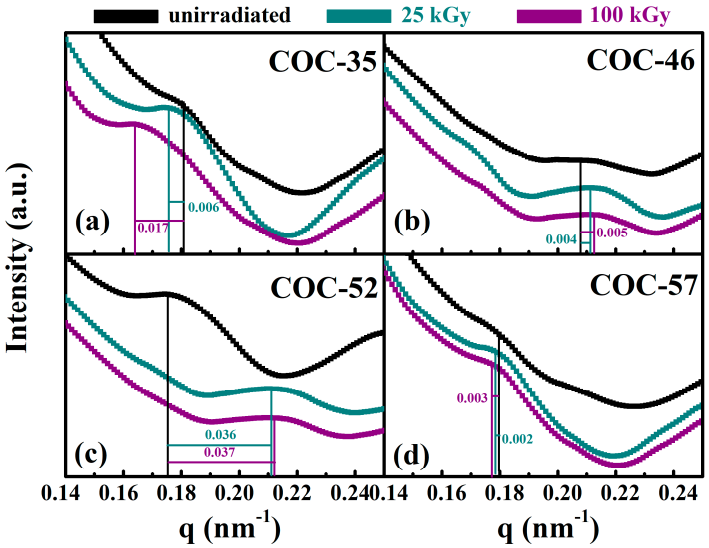



**Figure 8.** SAXS scattering intensity curves of COC with different norbornene contents. (**a**) COC-35: with norbornene content of 35%; (**b**) COC-46: with norbornene content of 46%; (**c**) COC-52: with norbornene content of 52%; (**d**) COC-57: with norbornene content of 57%.

The q-value of COC-52 closely resembles those of COC-35 and COC-57, while its irradiated q-value becomes comparable to COC-46. COC-52 contains approximately 52% norbornene, and its molecular structure exhibits a nearly 1:1 ratio between rigid norbornene rings and flexible chain segments. This composition gives rise to a unique semi-loose packing arrangement in the pristine state, where the presence of rigid cyclic units significantly hinders the tight stacking of molecular chains. As a result, the material develops enlarged free volume and pronounced nanoscale heterogeneity—structural characteristics that manifest as a relatively low initial q-value in SAXS measurements.

The relationship between the scattering vector q, the diffraction angle θ, and the wavelength of the incident X-ray is given by $q = (4\pi/\lambda) \sin\theta$. As the irradiation dose increases, the scattering peak gradually shifts towards larger value of q. Using the Bragg formula: $L = 2\pi/q_{max}$, the long-period results can be calculated, as shown in Table 1. With increasing dose, the long-period of COC samples slightly decrease. This decrease is attributed to the partial breakage of molecular chains caused by irradiation, particularly in the amorphous regions, resulting in shorter molecular chains that are more prone to rearrangement. Consequently, the statistical average distance, or long period, decreases. In contrast, COC-35, which has a high ethylene content, generates numerous flexible chain segments with free radicals during irradiation. These free radical reactions primarily lead to crosslinking and entanglement of the chain segments, accounting for the observed increasing trend in the long period of COC-35 with the absorbed dose.

The Guinier approximation indicates that at low values of q, the scattering curve can be represented by a specific formula, where $R_g$ is the radius of gyration and $I_{(0)}$ represents the intensity at the zero scattering angle (q = 0). To further investigate the structural changes in COC after irradiation, the SAXS curves for COC samples subjected to different absorbed doses were analyzed using the Guinier formula, allowing for the calculation of the radius

of gyration ($R_g$) for COC irradiated at various doses. The radius of gyration is defined as the root-mean-square distance between each electron in the particle and its center of mass, providing an indication of the average particle size within the sample. The expression for Guinier's formula is given in Equation (2):

$$I(q) = I_e M n^2 \exp\left(-\frac{\lambda^2 R_g^2}{3}\right) \quad (2)$$

The exponential term in the Guinier approximation, derived from linearly fitting ln(I) against $q^2 R_g{}^2$, is known as the Guinier plot. The specific region selected for this linear fitting is called the "Guinier region". The $R_g$ value is calculated from the slope of the fitted line ($k$) using Equation (3):

$$R_g = \sqrt{(-3k)} \quad (3)$$

Figure 9 presents the Guinier plot of COC samples that have been irradiated at various doses. As the absorbed dose increases, the absolute value of the slope of the fitted line decreases. The calculated results of gyration are summarized in Table 4. Among the four COCs, sample COC-35 exhibits the highest $R_g$ value. This implies that the entanglement of cross-linked structures in COC-35 causes a decrease in the average size of the internal particles and an increase in the mean statistical distance.

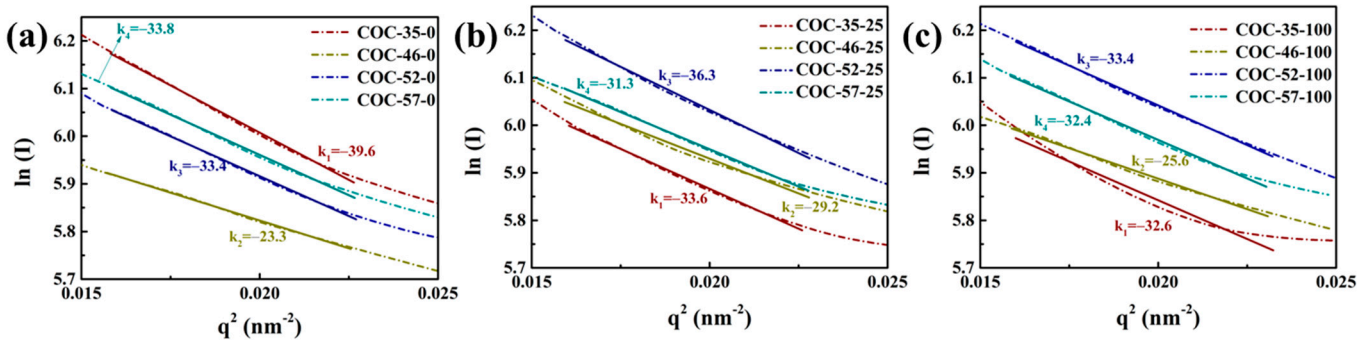



**Figure 9.** Guinier curves of COC with different norbornene content (**a**–**c**).

**Table 4.** Internal structural parameters of COC before and after irradiation.

| Sample | | Long Period (nm) | $R_g$ (nm) |
|---|---|---|---|
| Norbornene 35 mol% | COC-35-0 | 35.2 | 10.9 |
| | COC-35-25 | 35.4 | 10.0 |
| | COC-35-100 | 38.1 | 9.9 |
| Norbornene 46 mol% | COC-46-0 | 29.8 | 8.4 |
| | COC-46-25 | 29.5 | 9.4 |
| | COC-46-100 | 29.5 | 8.8 |
| Norbornene 52 mol% | COC-52-0 | 35.1 | 10.0 |
| | COC-52-25 | 29.6 | 10.4 |
| | COC-52-100 | 29.5 | 10.0 |
| Norbornene 57 mol% | COC-57-0 | 35.4 | 8.4 |
| | COC-57-25 | 34.9 | 9.7 |
| | COC-57-100 | 34.9 | 9.9 |

As the absorbed dose increases, the content of tertiary alkyl radicals generated by cleavage of chemical bonds in COC-46, COC-52, and COC-57 also increases after irradiation. These radicals have restricted mobility and are less prone to recombination. Instead, they can react with oxygen to form minor oxidation products. As a result, this leads to an increase

in the average size of the internal particles and a decrease in the mean statistical distance. Figure 10 summarizes the structural changes in the COC chain segments, including the long-period and radius of gyration models of the internal particles after irradiation.

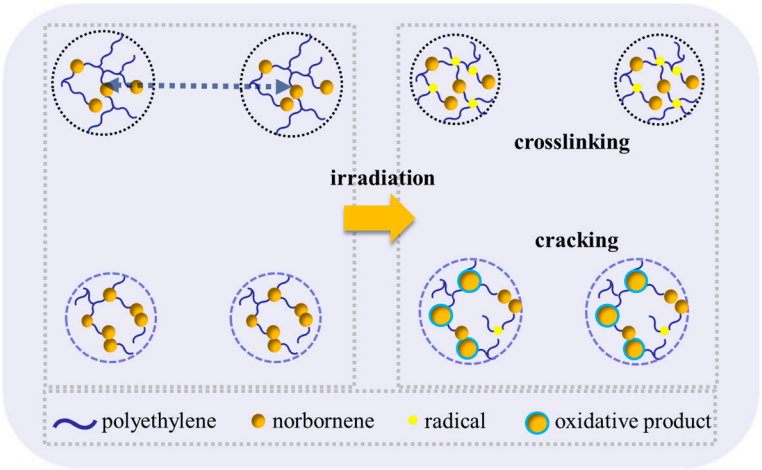



**Figure 10.** Relationship between norbornene content and microstructure in COC during irradiation.

In COC-35-100 and COC-46-100 systems with low norbornene content, the emergence of a characteristic signal at 0.71 ppm in NMR spectra reveals two distinct radiation-induced mechanisms. High-energy irradiation may trigger molecular chain crosslinking, bringing norbornene units into closer proximity and altering the electronic environment of bridge hydrogens, thereby shifting their chemical displacement upfield to 0.71 ppm. Simultaneously, γ-ray-induced radical reactions could promote branching and crosslinking in flexible chain segments, with newly formed terminal methyl protons overlapping with the shifted bridge hydrogens at 0.71 ppm. These chemical transformations correlate closely with the structural evolution observed by SAXS. For instance, COC-35 initially exhibits the largest $R_g$, but irradiation-induced crosslinking reduces particle size, which directly corresponds to the enhanced peak at 0.71 ppm in NMR spectra. In contrast, COC-46 undergoes oxidation due to the limited recombination of tertiary alkyl radicals generated by chain scission, leading to an increased $R_g$, while no significant enhancement in crosslinking signal is detected by NMR. For high-norbornene-content systems (COC-52-100 and COC-57-100), steric hindrance in rigid segments severely restricts radical migration and recombination, making β-scission the dominant degradation pathway. This manifests weakly in NMR spectra as minimal or even slightly reduced signal intensity at 0.7 ppm for COC-57, while SAXS shows a general increase in $R_g$, reflecting expansion of particulate dimensions due to oxidative degradation of the backbone. The combined NMR and SAXS analysis demonstrates that chain scission in rigid segments directly contributes to mesoscale structural expansion. In amorphous resins, changes in spatial-scale density fluctuations detected by SAXS correlate with chemical bond modifications revealed by NMR. For COCs, irradiation-induced chain scission shortens amorphous chains and may induce rearrangement, reducing long-period spacing. In ethylene-rich COC-35, however, crosslinking between flexible segments dominates, increasing long-period spacing instead. These structural changes find molecular-level correspondence: crosslinking networks are evidenced by altered bridge hydrogen environments in NMR, while chain scission is reflected in decreased peak intensity. By integrating NMR and SAXS observations, a clear pattern emerges: Low-norbornene COCs primarily undergo radical migration-mediated crosslinking and particle contraction, whereas high-norbornene COCs degrade predominantly via β-scission-induced backbone dissociation and particle expansion. This structure–degradation relationship elucidates the critical role of chemical composition in determining radiation stability.

## 4. Conclusions

Gamma irradiation induces free radical formation and migration in COCs, leading to significant polymer chain reorganization. Combined $^{1}H$ and $^{13}C$ NMR analysis reveals enhanced entanglement of flexible chain segments in COC-35. Conversely, COC samples containing 57 mol% norbornene exhibit attenuated multicomponent signals in NMR spectra, indicating that radical mobility is substantially restricted within the rigid cyclic structures, ultimately leading to chain scission. SAXS data corroborate these findings, demonstrating post-irradiation chain entanglement and—notably for high-norbornene COCs—increased particle size caused by radiation-induced oxidation products.

Collectively, these NMR and SAXS analyses systematically elucidate how the norbornene content dictates the radiation-induced structural evolution in COCs, thus refining our understanding of the effects of gamma radiation on COCs with different norbornene compositions.

**Supplementary Materials:** The following supporting information can be downloaded at: https://www.mdpi.com/article/10.3390/polym17131751/s1, Figure S1. ESR spectra of COCs with different norbornene contents, HDPE, and COP after irradiation: (a) absorbed dose of 25 kGy, (b) absorbed dose of 100 kGy. (c) Types of free radicals generated by irradiation in COCs with varying norbornene contents, HDPE, and COP; Figure S2. Comparative analysis of 1H NMR (measured at 50 °C) spectral assignments for COC-46 pre- and post-irradiation. The relative integral area for each signal (normalized to total spectral integral of 100%) is tabulated above the corresponding spectra; Figure S3. Comparative analysis of 1H NMR (measured at 50 °C) spectral assignments for COC-52 pre- and post-irradiation. The relative integral area for each signal (normalized to total spectral integral of 100%) is tabulated above the corresponding spectra; Figure S4. Comparative analysis of 1H NMR (measured at 50 °C) spectral assignments for COC-52 pre- and post-irradiation. The relative integral area for each signal (normalized to total spectral integral of 100%) is tabulated above the corresponding spectra; Figure S5. DSC curves of (a) COC-35, (b) COC-46, (c) COC-52, and (d) COC-57: comparison between pre- and post-irradiation states. References [43–45] are cited in Supplementary Materials.

**Author Contributions:** F.Z.: conducted the NMR and SAXS tests and wrote the manuscript; H.L. (Heng Lei), F.G., W.L. and J.H.: carried out the irradiation experiments; H.L. (Haiming Liu): suggested high-temperature NMR study and guided manuscript revision; Q.W.: performed the high-temperature $^{1}H$ NMR experiments; Z.X.: designed the experimental program and revised the manuscript; G.W.: designed the experimental program and revised the manuscript. All authors have read and agreed to the published version of the manuscript.

**Funding:** The work was supported by the National Natural Science Foundation of China (22176194).

**Institutional Review Board Statement:** Not applicable.

**Data Availability Statement:** The original contributions presented in the study are included in the article/Supplementary Materials; further inquiries can be directed to the corresponding authors.

**Conflicts of Interest:** The authors declare that they have no known competing financial interests or personal relationships that could have appeared to influence the work reported in this paper.

## References

1. Floros, G.; Saragas, N.; Paraskevopoulou, P.; Psaroudakis, N.; Koinis, S.; Pitsikalis, M.; Hadjichristidis, N.; Mertis, K. Ring Opening Metathesis Polymerization of Norbornene and Derivatives by the Triply Bonded Ditungsten Complex Na[$W_2(\mu$-$Cl)_3Cl_4(THF)_2$]·$(THF)_3$. *Polymers* **2012**, *4*, 1657–1673. [CrossRef]
2. Cui, J.; Yang, J.; Li, Y.; Li, Y. Synthesis of High Performance Cyclic Olefin Polymers (COPs) with Ester Group via Ring-Opening Metathesis Polymerization. *Polymers* **2015**, *7*, 1389–1409. [CrossRef]
3. Lamonte, R.R.; Mcnallu, D. Uses and processing of cyclic olefin copolymers. *Plast. Eng.* **2000**, *56*, 51–55.
4. Lago, W.S.R.; Aymes-Chodur, C.; Ahoussou, A.P.; Yagoubi, N. Physico-chemical ageing of ethylene–norbornene copolymers: A review. *J. Mater. Sci.* **2017**, *52*, 6879–6904. [CrossRef]

5. Barakat, H.; Lago, W.S.R.; Aymes-Chodur, C.; Ahoussou, A.P.; Yagoubi, N. Multi detection in Size-Exclusion Chromatography of electron beam irradiated Ethylene Norbornene Copolymers. *Polym. Degrad. Stab.* **2017**, *147*, 206–214. [CrossRef]
6. Šećerov, B.; Marinović-Cincović, M.; Popović, S.; Nedić, Z.; Kačarević-Popović, Z. Characterization of Gamma Irradiated Ethylene-Norbornene Copolymer using FTIR, UV-Vis and DSC Techniques. *Polym. Bull.* **2008**, *60*, 313–322. [CrossRef]
7. Zhang, F.; Dong, C.; Lei, H.; Guo, F.; Shen, R.; Xing, Z.; Wu, G. Effects of gamma radiation on cyclic olefin copolymers with varied norbornene content: Impacts on structure and properties at sterilization doses. *Polym. Degrad. Stab.* **2024**, *227*, 110881. [CrossRef]
8. Zhang, F.; Ji, Z.; Zhang, Q.; Shen, R.; Xing, Z.; Wu, G. Electron spin resonance study on free radicals in cyclic olefin copolymers irradiated by gamma rays at cryogenic and room temperatures. *Radiat. Phys. Chem.* **2022**, *202*, 110505. [CrossRef]
9. Zhang, F.; Mao, X.; Lei, H.; Guo, F.; Shen, R.; Xing, Z.; Wu, G. Investigation on discoloration mechanism of cyclic olefin copolymer under ionizing irradiation sterilization. *Polym. Degrad. Stab.* **2024**, *221*, 110676. [CrossRef]
10. Zhu, Q.; Fumitaka, H. The Effect of irradiation on a change in quantity of two types of radiation induced cross-links in HDPE with different morphology. *J. Radiat. Res. Radiat. Process.* **1990**, *8*, 80–85.
11. Kaminsky, W.; Spiehl, R. Copolymerization of cycloalkenes with ethylene in presence of chiral zirconocene catalysts. *Die Makromol. Chem.* **1989**, *190*, 515–552. [CrossRef]
12. Wang, W.; Qu, S.; Li, X.; Chen, J.; Guo, Z.; Sun, W. Transition metal complex catalysts promoting copolymers of cycloolefin with propylene/higher olefins. *Coord. Chem. Rev.* **2023**, *494*, 215351. [CrossRef]
13. Wendt, R.A.; Fink, G. Ethene-norbornene copolymerizations using two different homogeneous metallocene catalyst systems and investigations of the copolymer microstructure. *J. Mol. Catal. A Chem.* **2003**, *203*, 101–111. [CrossRef]
14. Yao, Z.; Lv, F.; Liu, S.-J.; Cao, K. Synthesis of ethylene and norbornene copolymer with metallocene catalysts and characteristic analysis. *J. Appl. Polym. Sci.* **2008**, *107*, 286–291. [CrossRef]
15. Blank, F.; Janiak, C. Metal catalysts for the vinyl/addition polymerization of norbornene. *Coord. Chem. Rev.* **2009**, *253*, 827–861. [CrossRef]
16. Heinz, B.S.; Alt, F.P.; Heitz, W. Pd(II)-catalyzed vinylic polymerization of norbornene and copolymerization with norbornene and copolymerization with norbornene carboxylic acid esters. *Macromol. Rapid Commun.* **1998**, *19*, 251–256. [CrossRef]
17. Li, Y.; Gao, M.; Wu, Q. Vinyl polymerization of norbornene by nickel (II) complexes bearing β-diketiminate ligands. *Appl. Organomet. Chem.* **2007**, *21*, 965–969. [CrossRef]
18. Suslov, D.S.; Bykov, M.V.; Abramov, P.A.; Pakhomova, M.V.; Ushakov, I.A.; Voronov, V.K.; Tkach, V.S. Synthesis, characterization, and application for addition polymerization of norbornene of novel acetylacetonate bis(anilines) palladium (II) complexes. *Inorg. Chem. Commun.* **2016**, *66*, 1–4. [CrossRef]
19. Wang, Y.-Y.; Lin, S.-A.; Zhu, F.-M.; Gao, H.-Y.; Wu, Q. Dinuclear nickel (II) complexes bearing two pyrazolylimine ligands: Synthesis characterization, and catalytic properties for vinyl-type polymerization of norbornene. *Eur. Polym. J.* **2008**, *44*, 2308–2317. [CrossRef]
20. Tosi, C.; Ciampelli, F.; Cameli, N. Spectroscopic examination of ethylene–propylene–norbornenic diene terpolymers. *J. Appl. Polym. Sci.* **1972**, *16*, 801–810. [CrossRef]
21. Herfert, N.; Montag, P.; Fink, G. Elementary processes of the Ziegler catalysis, 7. Ethylene, α-olefin and norbornene copolymerization with the stereorigid catalyst systems ipr[flucp]zrcl$_2$/mao and me$_2$si[ind]$_2$zrcl$_2$/mao. *Macromol. Chem. Phys.* **2001**, *194*, 3167–3182. [CrossRef]
22. Ruchatz, D.; Fink, G. Ethene−Norbornene Copolymerization Using Homogenous Metallocene and Half-Sandwich Catalysts: Kinetics and Relationships between Catalyst Structure and Polymer Structure. 2. Comparative Study of Different Metallocene- and Half-Sandwich/Methylaluminoxane Catalysts and Analysis of the Copolymers by $^{13}$C Nuclear Magnetic Resonance Spectroscopy. *Macromolecules* **1998**, *31*, 4674. [CrossRef]
23. Monti, G.A.; Acosta, R.H.; Chattah, A.K.; Linck, Y.G. Solid state nuclear magnetic resonance of polymers. *J. Magn. Reson. Open* **2023**, *16–17*, 100119. [CrossRef]
24. Provasoli, A.; Ferro, D.R.; Tritto, I.; Boggioni, L. The Conformational Characteristics of Ethylene−Norbornene Copolymers and Their Influence on the 13C NMR Spectra. *Macromolecules* **1999**, *32*, 6697–6706. [CrossRef]
25. Shin, J.Y.; Park, J.Y.; Liu, C.; He, J.; Kim, S.C. Chemical structure and physical properties of cyclic olefin copolymers (IUPAC Technical Report). *Pure Appl. Chem.* **2005**, *77*, 801–814. [CrossRef]
26. Tritto, I.; Marestin, C.; Boggioni, L.; Zetta, L.; Provasoli, A.; Ferro, D.R. Ethylene−Norbornene Copolymer Microstructure. Assessment and Advances Based on Assignments of 13C NMR Spectra†. *Macromolecules* **2000**, *33*, 8931. [CrossRef]
27. Tritto, I.; Marestin, C.; Boggioni, L.; Sacchi, M.C.; Brintzinger, H.H.; Ferro, D.R. Stereoregular and Stereoirregular Alternating Ethylene−Norbornene Copolymers. *Macromolecules* **2001**, *34*, 5770–5777. [CrossRef]
28. Fernández-Delgado, S.; García-Peñas, A.; Serrano, D.; Cerrada, M.L.; Gómez-Elvira, J.M. Detailed microstructure analysis through monomeric insertion modes of poly(propylene-co-norbornene) copolymers and poly(propylene-co-ethylene-co-norbornene) terpolymers with low norbornene contents. *Polym. Test.* **2023**, *124*, 108081. [CrossRef]

29. Gao, H.; Chen, S.; Du, B.; Dai, Z.; Lu, X.; Zhang, K.; Pan, L.; Li, Y.; Li, Y. Cyclic olefin copolymers containing both linear polyethylene and poly(ethylene-co-norbornene) segments prepared from chain shuttling copolymerization of ethylene and norbornene. *Polym. Chem.* **2022**, *13*, 245–257. [CrossRef]
30. Bykov, V.I.; Butenko, T.A. Composition and Microstructure of Norbornene–Ethylene Copolymers. *Polym. Sci. Ser. B* **2018**, *60*, 754–759. [CrossRef]
31. Rische, T.; Waddon, A.J.; Dickinson, L.C.; MacKnight, W.J. Microstructure and Morphology of Cycloolefin Copolymers. *Macromolecules* **1998**, *31*, 1871–1874. [CrossRef]
32. Mortazavi, S.M.M.; Galland, G.B.; Khonakdar, H.; Ahmadjo, S.; Hayati, S. Effect of chain transfer agent on microstructure and thermal properties of cyclic olefin copolymer with low comonomer content. *J. Therm. Anal. Calorim.* **2022**, *147*, 13341–13350. [CrossRef]
33. Brar, A.S.; Kumar, R. Investigation of microstructure of the N-vinyl-2-pyrrolidone/methyl methacrylate copolymers by NMR spectroscopy. *J. Appl. Polym. Sci.* **2002**, *85*, 1328–1336. [CrossRef]
34. Boggioni, L.; Losio, S.; Tritto, I. Microstructure of Copolymers of Norbornene Based on Assignments of 13C NMR Spectra: Evolution of a Methodology. *Polymers* **2018**, *10*, 647. [CrossRef]
35. Arndt, M.; Beulich, I. $C_1$-symmetric metallocenes for olefin polymerisation, 1. Catalytic performance of [$Me_2C$(3-$^{tert}$BuCp)(Flu)]$ZrCl_2$ in ethene/norbornene copolymerization. *Macromol. Chem. Phys.* **1998**, *199*, 1221–1232.
36. Wendt, R.A.; Fink, G. $^{13}$C NMR Studies of Ethene/Norbornene Copolymers using $^{13}$C-Enriched Monomers: Signal Assignments of Copolymers Containing Norbornene Microblocks of up to a Length of Three Norbornene Units. *Macromol. Chem. Phys.* **2001**, *202*, 3490–3501. [CrossRef]
37. Viglianisi, C.; Menichetti, S.; Assanelli, G.; Sacchi, M.C.; Tritto, I.; Losio, S. Ethylene/hindered phenol substituted norbornene copolymers: Synthesis and NMR structural determination. *J. Polym. Sci. Part A Polym. Chem.* **2012**, *50*, 4647–4655. [CrossRef]
38. Hai, Y.; Huang, C.; Ma, M.; Liu, Q.; Wang, Y.; Liu, Y.; Tian, F.; Lin, J.; Zhu, Z. SAXS investigation of latent track structure in HDPE irradiated with high energy Fe ions. *Nucl. Instrum. Methods Phys. Res. Sect. B Beam Interact. Mater. At.* **2015**, *356–357*, 129–134. [CrossRef]
39. Fayolle, B.; Verdu, J. Radiation aging and chemi-crystallization processes in polyoxymethylene. *Eur. Polym. J.* **2011**, *47*, 2145–2151. [CrossRef]
40. Somani, R.H.; Hsiao, B.S.; Nogales, A.; Srinivas, S.; Tsou, A.H.; Sics, I.; Balta-Calleja, F.J.; Ezquerra, T.A. Structure development during shear flow-induced crystallization of i-PP: In-situ small-angle X-ray scattering study. *Macromolecules* **2000**, *33*, 9385–9394. [CrossRef]
41. Rui, E.; Yang, J.; Li, X.; Ma, G. Effect of proton irradiation on mechanical properties of low-density polyethylene/multiwalled carbon nanotubes composites. *Polym. Compos.* **2014**, *36*, 278–286. [CrossRef]
42. Ge, L.; Wang, D.-X.; Xing, R.; Ma, D.; Walsh, P.J.; Feng, C. Photoredox-Catalyzed Oxo-Amination of Aryl Cyclopropanes. *Nat. Commun.* **2019**, *2019*, 4367. [CrossRef] [PubMed]
43. Zhao, Y.; Wang, M.; Tang, Z.; Wu, G. ESR study of free radicals in UHMW-PE fiber irradiated by gamma rays. *Radiat. Phys. Chem.* **2010**, *79*, 429–433. [CrossRef]
44. Kiminami, H.; Imae, Y.; Takahashi, E.; Wei, H.; Oomura, S.; Abe, Y. Electron beam sterilization of cyclo olefin polymer leads to polymer degradation and production of alkyl radicals. *J. Appl. Polym. Sci.* **2016**, *133*, 43498. [CrossRef]
45. Mochizuki, A.; Ono, D.; Kiminami, H.; Shinoda, S.; Abe, Y. Carbon radicals generated by solid polymers: Electron spin resonance spectroscopy for detection of species in water. *J. Appl. Polym. Sci.* **2019**, *137*, 48604. [CrossRef]


**Disclaimer/Publisher's Note:** The statements, opinions and data contained in all publications are solely those of the individual author(s) and contributor(s) and not of MDPI and/or the editor(s). MDPI and/or the editor(s) disclaim responsibility for any injury to people or property resulting from any ideas, methods, instructions or products referred to in the content.